Fast and Accurate Transient Analysis of Large Grounding Systems in Multilayer Soil

Blagoja Markovski, Leonid Grcev, *Life Fellow, IEEE*, and Vesna Arnautovski-Toseva

***Abstract*—One of the most accurate approaches to the lightning-related transient analysis of grounding systems in layered soil is based on the method of moments solution of the integral form of the Maxwell equations. The practical application of this rigorous model to large systems is hindered by a great amount of computer time required for the numerical integration of oscillatory and slowly convergent Sommerfeld integrals (SI). As a result, approximate methods that avoid the solution of SI, e.g., image theory-based methods, are often used for computation of the response of large grounding systems. In this article, we extend the application of the rigorous model for large grounding systems in multilayered soil by applying a procedure that minimizes the number of direct computations of the SI using interpolation over a grid of a small number of sample points. We implement a three-dimensional interpolation scheme that adapts to the problem to minimize the interpolation grid, maintaining the accuracy of the rigorous approach. The developed model is applied for the analysis of transient voltages that might couple to secondary cables and disrupt the operation of connected equipment in case of lightning. The analysis shows that there are cases when the image theory-based models might underestimate the possibly harmful transient voltages.**

***Index Terms*—Electromagnetic analysis, integral equations, frequency response, green functions, grounding, interpolation, modeling.**

I. Introduction

GROUNDING grids are the most effective solution for safety and protection in large substations and plants in case of disturbances, such as power faults or lightning [1]. Since such disturbances might have a high-frequency content, methods for analysis in wide frequency ranges are necessary. Several accurate numerical procedures are applied for this purpose, such as the method of moments (MoM) [2]–[5], the finite element method [6], and the finite difference time domain method [7]. Among these approaches, the MoM-based approach is a preferred choice for modeling large and complex grounding systems [8]–[10].

Manuscript received November 11, 2019; revised February 11, 2020; accepted March 23, 2020. Date of publication April 10, 2020; date of current version March 24, 2021. Paper no. TPWRD-01294-2019. *(Corresponding author: Blagoja Markovski.)*

Blagoja Markovski and Vesna Arnautovski-Toseva are with the Faculty of Electrical Engineering and Information Technologies, Ss. Cyril and Methodius University, 1000, Skopje, Macedonia (e-mail: bmarkovski@feit.ukim.edu.mk; atvesna@feit.ukim.edu.mk).

Leonid Grcev is with the Macedonian Academy of Sciences and Arts, 1000, Skopje, Macedonia (e-mail: Leonid.Grcev@ieee.org).

Color versions of one or more of the figures in this article are available online at https://ieeexplore.ieee.org.

Digital Object Identifier 10.1109/TPWRD.2020.2985926

The MoM [11] is developed from the antenna theory and is suitable for high-frequency and fast transient analysis (latter via Fourier transform techniques) [3], [4]. MoM solves an integral form of Maxwell equations with Green's functions that are based on an exact mathematical solution of the electromagnetic fields of an electric dipole in the earth [12], [13]. The accuracy of computer models based on this rigorous method, e.g., [3], [4], has been validated through comparisons with published experimental results by several independent research groups (see [14]–[16]). Olsen *et al*. [5] have established this approach as an "exact" solution to this problem and as a "gold standard" for comparisons.

However, the excessive amount of computer time required to compute the Green's functions, which includes numerical integration of oscillatory and slowly convergent Sommerfeld integrals (SI) [13], hinders the practical application of this rigorous approach. As a result, computations of the response of large grounding systems were usually made using approximate models that avoid computations of SI, e.g., by applying image theory-based methods [8]–[10], [17]. This is, even more, a problem in a multilayer model of soil, which is required for a more precise analysis [18]. There have been efforts for rigorous modeling of grounding systems in multilayer soil in a wide frequency range, but computations of only small and simple grounding systems have been reported [19]–[21].

Efficient techniques based on interpolation that minimize direct evaluation of SI were developed in the antenna theory, first for a uniform model of soil [22], and later for multilayer media [23], [24]. SI are first pre-computed in a suitable small grid of points, and all required values are later calculated by interpolation between the grid points.

In this paper, we apply an interpolation procedure that adapts the interpolation grid to the analyzed case, which reduces the number of direct computations of the Sommerfeld integrals while maintaining the accuracy of the rigorous approach. We apply the MoM technique for the numerical solution of the mixed-potential integral equation (MPIE) developed by Harrington [11]. It has been shown that MPIE is well suited for analysis in layered media [25]. However, the choice of MPIE requires a different choice of potentials than the standard one introduced by Sommerfeld [12]. In this paper, we adopt the so-called "formulation C," which is preferable for structures with arbitrarily oriented electrodes that penetrate different layers [26].

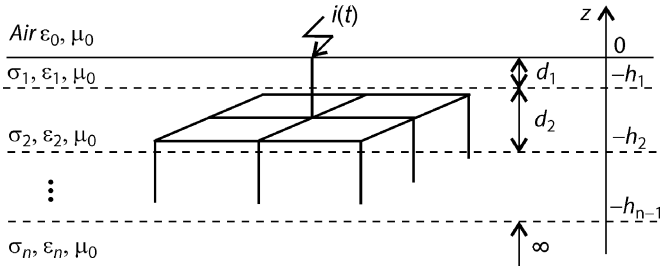

Fig. 1. Grounding system in multilayer soil energized by a current impulse.

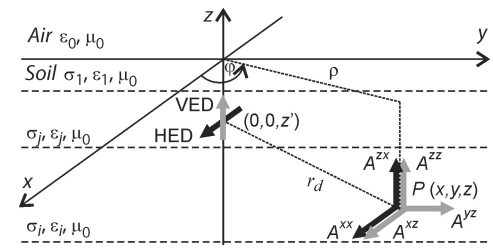

Fig. 2. Components of the magnetic vector potential $\vec{A}$ for the horizontal (HED) and vertical electric dipole (VED) in the "formulation C."

II. Mixed Potential Integral Equation and Method of Moments

A horizontally stratified multilayer soil with plane boundaries is illustrated in Fig. 1. Layers are characterized by conductivity σ_i, permittivity ε_i, and permeability of vacuum μ_0. Their thickness is d_i, except for the bottommost semi-infinite layer. The grounding system is assumed to comprise a network of straight thin cylindrical metallic conductors with an equivalent circular cross-section in an arbitrary position, possibly penetrating different layers.

The transient problem is first solved by a formulation in the frequency domain by computing the response to a steady-state, time-harmonic excitation for a wide range of frequencies starting at 0 Hz. The $e^{j\omega t}$ time variation is implicitly assumed throughout the paper. The time-domain response is then obtained by the application of a suitable Fourier inversion technique [4]. A detailed description of the method can be found elsewhere, e.g., [3], [4], [27], [28]. Here, we briefly summarize the main steps.

To approximate the longitudinal current distribution, the grounding electrodes are thought as divided into *N* fictitious segments, along which a constant longitudinal current I_n is assumed. As a result of the application of MoM [11], the MPIE is reduced to a matrix equation:

$$[Z] \cdot [I] = [V] \tag{1}$$

where [*I*] is a column matrix with unknown currents I_n, [*V*] is related to energization of the grounding system and [*Z*] is a square matrix of order *N* with elements:

$$Z_{mn} = \frac{\Delta \ell_m}{4\pi} \left(j\omega\mu_0 \int_{\ell'_n} \overline{\overline{G}}_A d\ell'_n - \frac{1}{\underline{\sigma}_i} \frac{\partial}{\partial \ell_m} \int_{\ell'_n} \frac{\partial}{\partial \ell'_n} G_\Phi d\ell'_n \right) \tag{2}$$

where *m* and *n* are numerals of grounding electrode segments and $\underline{\sigma}_i = \sigma_i + j\omega\varepsilon_i$ is complex conductivity of the *i-th* layer where the observation point is located. Segments are subject to thin-wire approximation, which allows for approximating filamentary current along *n-th* segment axis ℓ'_n and evaluation of the voltage along a line ℓ_m at the *m-th* segment surface parallel to its axis.

The grounding system can be energized in different ways, for example, by injection of current, which is illustrated in Fig. 1. The interested reader can find details for this and other types of energization in [29]. A solution of (1) determines the I_n, which allows for evaluation of all required grounding system characteristics [4].

The key step is to determine $\overline{\overline{G}}_A$ and G_Φ in (2), which are dyadic Green's function for the magnetic vector potential and Green's function for the electric scalar potential, respectively.

III. Green's Functions

Green's functions (GF) in layered media are usually expressed in terms of components of a horizontal electric dipole (HED) (pointed to x-direction) and vertical electric dipole (VED) (pointed to z-direction) in a local coordinate system, as shown in Fig. 2. The choice of potentials according to "formulation C" implies the following elements of the dyadic GF of the magnetic vector potential:

$$\begin{aligned} \overline{\overline{G}}_A = (\ell'_x \ell_x + \ell'_y \ell_y) G_A^{xx} + \ell'_x \ell_z G_A^{zx} + \ell'_y \ell_z G_A^{zy} + \\ \ell'_z \ell_x K_A^{xz} + \ell'_z \ell_y K_A^{yz} + \ell'_z \ell_z K_A^{zz} \end{aligned} \tag{3}$$

where $\ell'_{x,y,z}$ and $\ell_{x,y,z}$ are direction cosines of ℓ'_n and ℓ_m. The meaning of the first superscript of the GF in (3) is the orientation of the magnetic vector potential at the point of observation, and the second superscript is the orientation of the source.

Once the choice of $\overline{\overline{G}}_A$ is made, GF for the electric scalar potential G_Φ follows from the Lorentz gauge [26]. The components of the GF are given in the Appendix.

IV. Evaluation of Sommerfeld Integrals by Adaptive Interpolation

Evaluation of integrals in (2) requires repeated computations of GF for the source and observation points in a volume determined by the geometry of the analyzed grounding system. GF depends on three geometric variables defined in the local coordinate system shown in Fig. 2, i.e., the radial distance between the source and observation points ρ, and the z-coordinates of the source and observation points z' and z. Therefore, it is possible to determine the corresponding Sommerfeld integrals by three-dimensional interpolation between pre-computed values in a suitable grid of points defined by these three variables [23], [24].

Here, we use a three-dimensional cubic interpolation, which requires pre-computed Sommerfeld integrals at 64 grid points surrounding the point where the result is required. The interpolation grid points are arranged around the observation point in

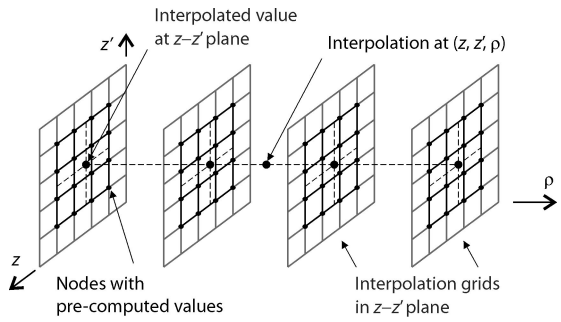

Fig. 3. Grid points arranged around the observation point in groups of 16 points at 4 equally spaced parallel z–z' planes perpendicular to a line that parallels the ρ-coordinate axis (adapted from [24]).

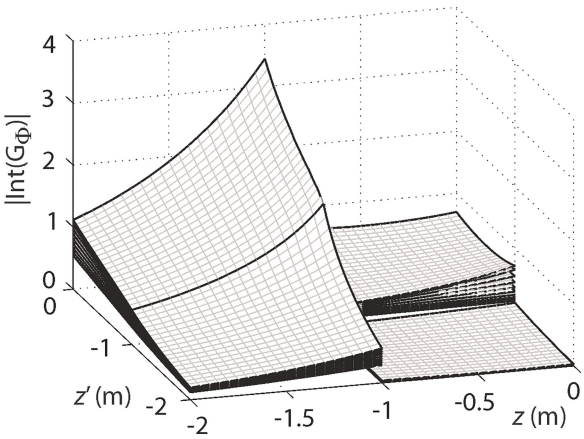

Fig. 4. Modulus of pre-computed values of the integral part of G_Φ (11) in z – z' planes for $0 > z, z' > -2$, for a depth of layer $d_1 = 1$ m, in interpolation grids in four regions. Planes are for 10 values of ρ in the range 0.1 m $< \rho <$ 3 m. $f =$ 1 MHz, $\sigma_1 = 0.01$ S/m, $\sigma_2 = 0.19$ S/m, $\varepsilon_{r1} = \varepsilon_{r2} = 10$, $\mu_1 = \mu_2 = \mu_0$.

groups of 16 points at 4 equally spaced parallel $z - z'$ planes perpendicular to a line that parallels the ρ-coordinate axis, as illustrated in Fig. 3. First, values at the intersecting points between the perpendicular line in the ρ-direction and the four $z - z'$ planes are computed by two-dimensional cubic interpolation [22]. Then the required value is computed by one-dimensional cubic interpolation from these four values (see Fig. 3). The five Green's functions (given in Appendix) are evaluated simultaneously on the same interpolation grid. The interpolation grids are adapted to the analyzed case by choosing only those nodes that will be used for interpolation.

The interpolation grids are divided into regions corresponding to a combination of layers where source and field points are located. The number of such regions is equal to m^2, where m is the number of layers. Fig. 4 illustrates a case of two-layer soil with four such regions. The density of the grid points depends on the frequency and soil characteristics. We have used a step for points in the $z - z'$ plane of $\min(\lambda_i/10,\ d_i/10)$ and for ρ-coordinate of $\lambda_i/10$ up to λ_i and $\lambda_i/4$ above λ_i, where λ_i is the wavelength in the *i-th* layer where the observation point is located.

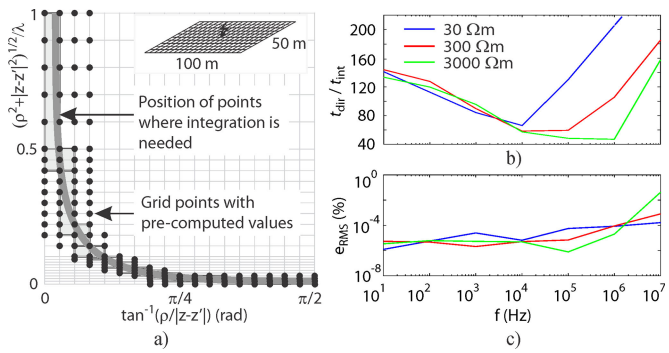

Fig. 5. a) Adaptive choice of grid points with pre-computed values of Sommerfeld integrals (SI) depending on the position of points where SI are needed. b) The ratio between times required for direct numerical integration of SI and proposed interpolation procedure of 50 m by 100 m grid in soil with three values of resistivity. c) RMS error for computation of currents.

The general form of SI is preconditioned for interpolation by extracting the singularities, which can be expressed in closed form (see Appendix). The resulting form of the SI is well-behaved for numerical evaluation and interpolation, which is illustrated in the example in Fig. 4.

V. Efficiency and Accuracy of the Proposed Interpolation Technique

The proposed procedure increases computational efficiency by minimizing the number of numerically integrated SI. The number of computations of SI depends on several factors, such as dimensions and geometry of the problem, number of segments, number and characteristics of layers, the number and range of frequencies required for time-domain transformation, and the number and type of computed quantities. As an example, Fig. 5(a) illustrates the reduction of the number of interpolation grid points by choosing only those that are used in a case of 100 m by 50 m grid with 200 meshes in uniform soil. Fig. 5(b) shows efficacy improvement and Fig. 5(c) accuracy in the analyzed case. Fig. 5(b) shows the ratio of the time required for direct numerical integration of SI during completing the MoM matrix equation (1) t_{dir} and time required when using the proposed interpolation technique t_{int}. The interpolation technique typically shortens the computation time by a factor of several tens to a few hundred. For convenience, we show results for the uniform soil model in Fig. 5, but shown improvement of efficacy and accuracy is typical also for multilayer soil.

We computed the RMS error $\varepsilon_{\mathrm{RMS}}$ for the longitudinal current along the grid conductors as follows [30]:

$$\varepsilon_{\mathrm{RMS}} = \left[\frac{\sum_{n=1}^{N} \left| I_n^{Int} - I_n^{Dir} \right|^2}{\sum_{n=1}^{N} \left| I_n^{Dir} \right|^2} \right]^{1/2} \cdot 100\ (\%) \qquad (4)$$

Here, I_n^{Dir} is the phasor of the segments' currents computed by direct numerical integration of SI and I_n^{Int} is the phasor of the currents got using the interpolation technique. N is the total number of segments in the grid. Fig. 5(c) shows a typical result for the error, which is smaller than 0.1 percent. We have tested the accuracy of this approach for the earth's resistivity from

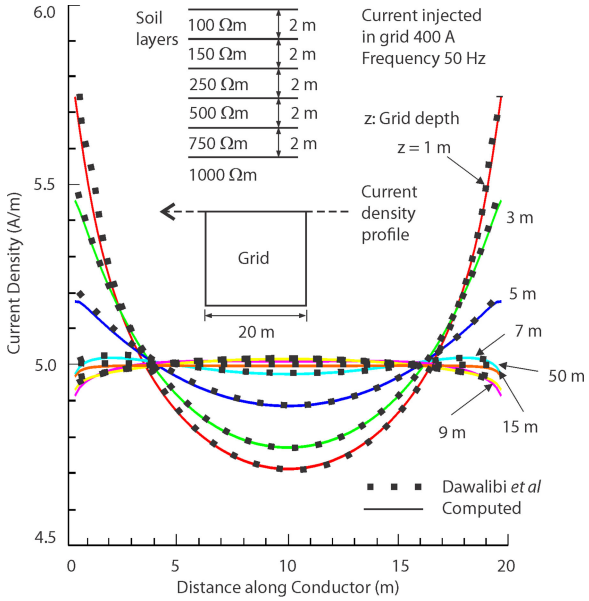

Fig. 6. Comparison with published data by Dawalibi *et al.* [18].

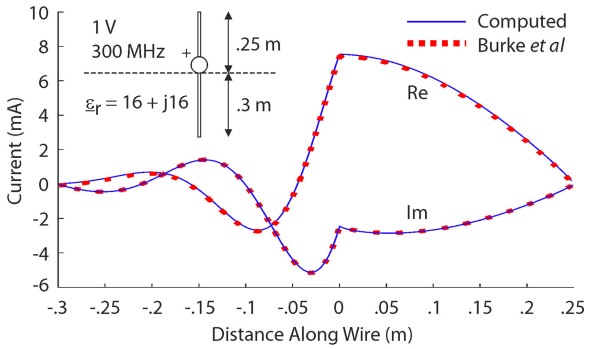

Fig. 7. Comparison with published data by Burke *et al.* [22], Fig. 3.

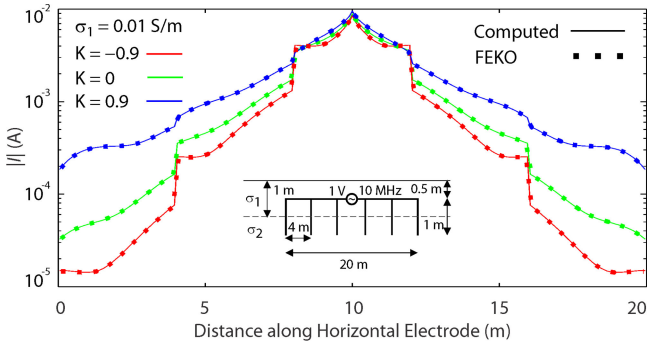

Fig. 8. Comparison with commercial full-wave electromagnetic software FEKO [31].

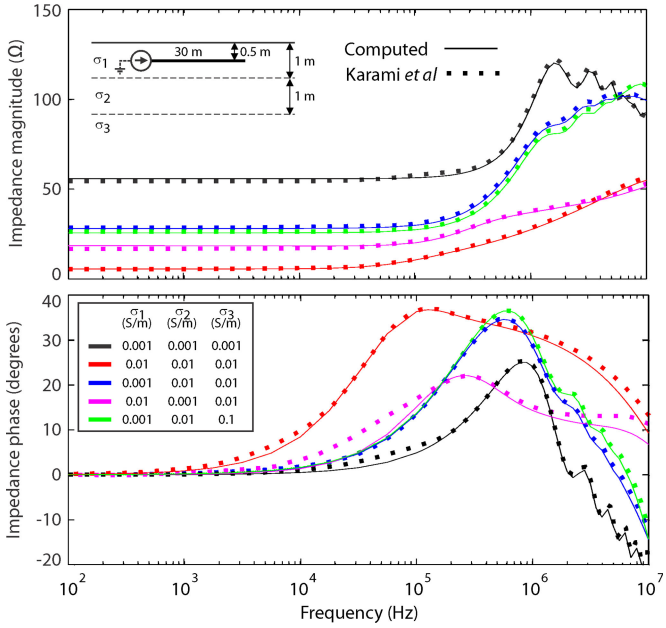

Fig. 9. Comparison with published data by Karami *et al.* [41].

10 Ωm to 3000 Ωm and the frequency in a range from 0 Hz to 10 MHz.

The choice of the interpolation technique and the density of the interpolation grids were made to maintain such accuracy. Further improvement of the efficiency is planned by more efficient methods for interpolation and application of accurate approximations.

VI. Comparison With Published Simulation and Experimental Data

In Fig. 6 we compare our computations with published results by Dawalibi *et al.* [18], for the current dissipated in the soil through a rectangular loop buried at various depths in a six-layer soil model.

Next, in Fig. 7 we compare our computations with the test case of a vertical wire that penetrates uniform earth published by Burke *et al.* [22].

In Fig. 8 we compare simulation results for the illustrated wire structure in a two-layer soil with the computed results by the commercial full-wave electromagnetic software FEKO. The 20-m long horizontal wire is buried at 0.5 m depth with 1-m long vertical rods at every 4 m. The upper soil layer has a thickness of 1 m and a conductivity of 0.01 S/m. Three different alternative values of the conductivity of the lower layer are 0.19 S/m ($K = -0.9$), 0.01 S/m ($K = 0$), and 0.000526 S/m ($K = 0.9$), where:

$$K = (\sigma_1 - \sigma_2) / (\sigma_1 + \sigma_2) . \tag{5}$$

Both layers have a relative permittivity 10 and permeability of vacuum. The energization is by serially connected voltage generator with an RMS value of 1 V at a frequency of 10 MHz.

The results of simulations in all cases in Figs. 6–8 are in good agreement with the published reference results.

In Fig. 9 we compare our simulation results of harmonic grounding impedance of a horizontal electrode energized by current injection in a three-layer soil with results in the recent publication by Karami *et al.* [41]. There are different methods to compute harmonic impedance; we have used the method introduced in 1997 in [8] and [42], where a quotient between phasors of the maximal value of the ground potential rise at the point of

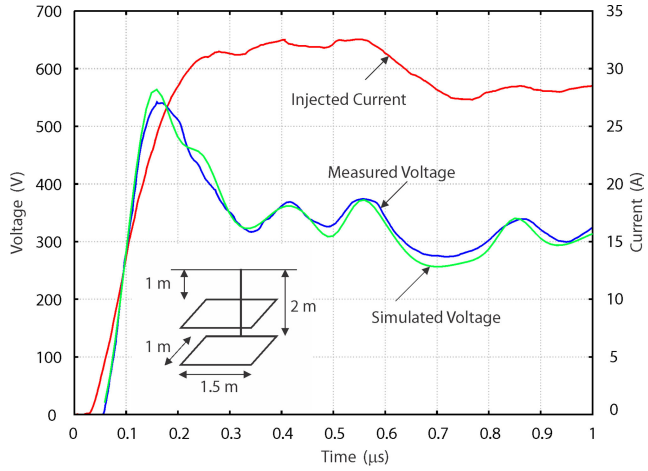

Fig. 10. Measured and simulated transient voltages to the remote ground and the injected current pulse at the feed point of the double-loop grounding system.

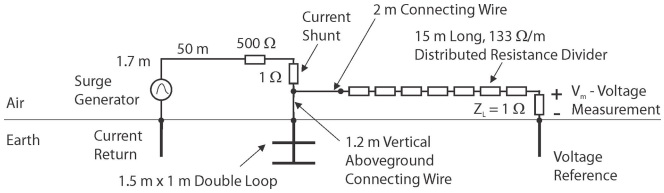

Fig. 11. Test electrode and the experimental setup (adapted from [29]).

current injection and the injected harmonic current defines the harmonic impedance. The comparison with the results based on the method proposed in [41] shows good agreement.

Finally, in Fig. 10 we compare our simulation with an experiment conducted by Electricite de France (EdF) in Les Renardieres, France, in 1978 [32], [33]. The case of the double-loop copper wire with a 6 mm radius, illustrated in Fig. 10, is used for the validation of the proposed simulation technique. The experimental setup used by EdF is illustrated in Fig. 11 (more details on the setup can be found elsewhere [16]). Fig. 10 shows the measured injected pulse current and transient voltage ([34, Fig. 3–19b]). Analysis in [16] has shown that simulated voltage has to be corrected for an added inductance of 1.2 μH of the connecting cables and a delay of 0.05 μs caused by the resistive divider. Interested readers can find a detailed analysis of the influence of the measurement circuit on the measured values in [16]. The apparent resistivity 70 Ωm of the soil is not measured separately but is estimated from the low-frequency values of the grounding harmonic impedance determined from the measured current and voltage pulses by application of the Fourier transform technique [32]. The relative permittivity of the soil of 15 is adopted by EdF as a typical value and is not measured separately [32], [33]. Fig. 10 shows that the simulated voltage between the feed point at the earth's surface and the voltage reference point is consistent with the measured results.

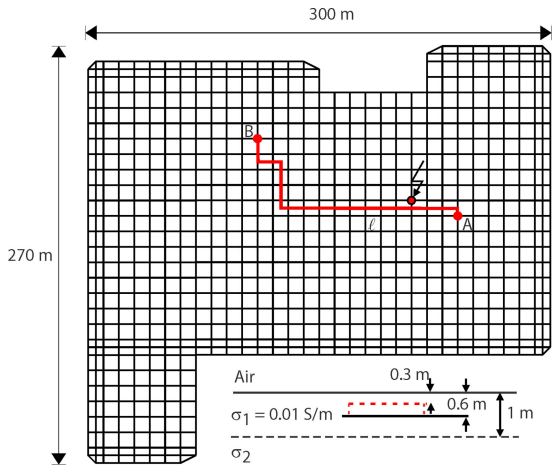

Fig. 12. The 500-kV grounding grid and path ℓ of a DC power supply cable between points A and B (adapted from [34]).

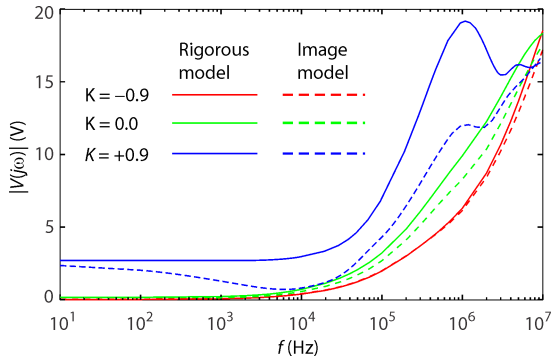

Fig. 13. Modulus of GPR frequency response at the current injection point for a harmonic injected current of 1 A for three cases of soil models computed by rigorous and image models.

VII. Numerical Examples: Transient Voltages in Large Grounding Grid in Case of Lightning

As an example, we analyze a large grounding grid, similar to the one analyzed in [34] (see Fig. 12). The buried depth of the grid is 0.6 m, and the conductors are made of copper with 0.007 m radius. The soil has two layers. The upper layer with a thickness of 1 m has a resistivity of 100 Ωm. We analyze three cases, when the lower layer has a resistivity of 5.26 Ωm (K = –0.9), 100 Ωm ($K = 0$), or 1900 Ωm ($K = 0.9$). Both layers have a relative permittivity 10 and permeability of vacuum. Fig. 12 shows a path ℓ between points A and B along which a DC power cable is laid. The path is laid at 0.3 m depth and terminates at points A and B at the grid conductors.

In this section, we compare the results of the proposed interpolation technique with an approximate model based on the image theory (the interested reader can find details of this approximate model in [35] and [36]). Since the accuracy of the interpolation technique is similar to the accuracy of the rigorous model, we refer to this approach in Fig. 13 and the following text as a "rigorous model". Also, we refer to the approximate approach as an "image model".

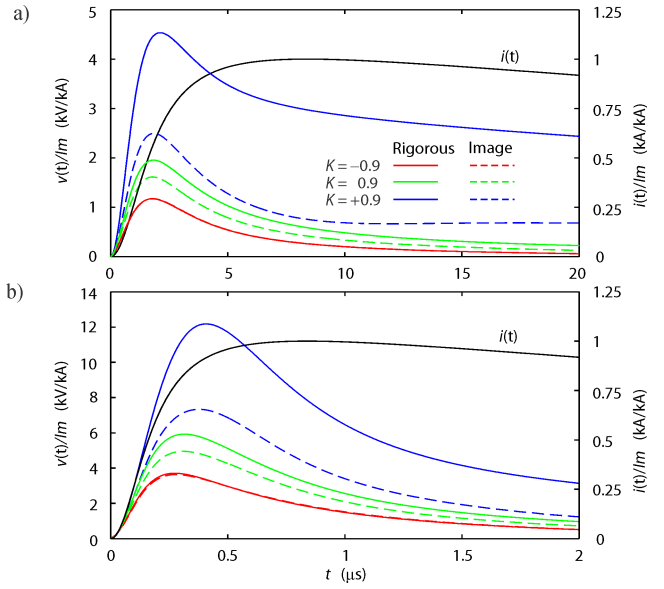

Fig. 14. Lightning current pulses and transient GPR (normalized to the current pulse peak value I_m) in three different two-layer soil models computed by rigorous and approximate models. a) First stroke: $T_1/T_2 = 8$ μs/80 μs. b) Subsequent stroke: $T_1/T_2 = 0.8$ μs/50 μs.

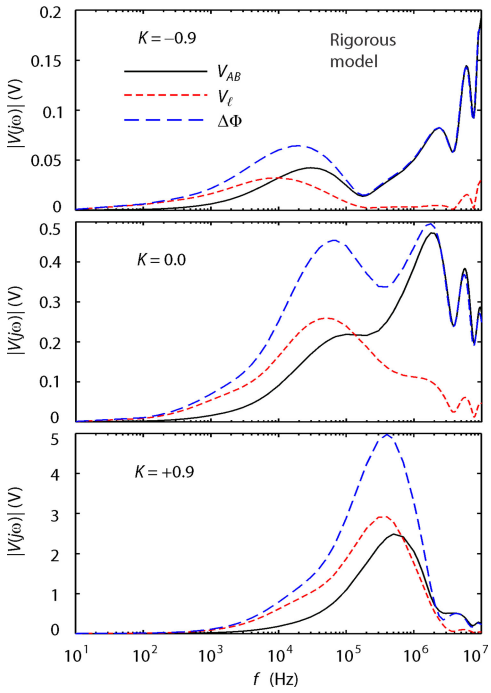

Fig. 15. Modulus of voltage along path ℓ between points A and B for three cases of two-layer soil computed by the rigorous model.

A. Ground Potential Rise at Current Injection Point

Fig. 13 shows the modulus of computed ground potential rise (GPR) $V(j\omega)$at the current injection point, for a harmonic injected current of 1 A and three cases of soil models. It is worth noting that for the injected harmonic current of $I(j\omega) = 1$ A, such as in the example in Fig. 13, the values are equivalent to the harmonic grounding impedance $Z(j\omega)$ in ohms, since $Z(j\omega) = V(j\omega)/I(j\omega)$.

The approximate model is consistent with the rigorous for the very conductive lower layer but underestimates GPR for the very resistive lower layer.

Figs. 14 shows transient GPR for lightning current waveforms typical of first and subsequent strokes. The two lightning current waveforms were chosen by Rachidi *et al.* [37] to fit experimental data corresponding to the typical first and subsequent return strokes, based on observations of Berger *et al.* [38]. The first stroke current pulse is characterized by a zero-to-peak time T_1 of about 8 μs and time-to-half-value T_2 of about 80 μs, whereas the subsequent stroke current has $T_1/T_2 = 0.8$ μs/50 μs. Fig. 14(a) shows current $i(t)$ of the first stroke and transient GPR $v(t)$ (both normalized to the current pulse peak value I_m) computed by the rigorous and image model. Fig. 14(b) shows results for subsequent stroke current. The approximate model largely underestimates voltages for the very resistive lower layer.

Execution time for computation of the transient GPR for each soil model by the interpolation technique was about one hour on a PC with Intel Core i7-4702MQ processor at 2.2GHz and 8 GB RAM. We expect that the planned optimization of the computer program will further reduce the execution time.

B. Voltage Along a Path Between Two Points at the Grid Conductors

The total voltage V_{AB} between points A and B along a path ℓ (see Fig. 12) may be expressed as a sum of two terms [39], [40]:

$$V_{AB} = (\Phi_A - \Phi_B) + \int_\ell \vec{A} \cdot d\vec{\ell} = \Delta\Phi + V_\ell \qquad (6)$$

where $\Delta\Phi = \Phi_A - \Phi_B$ is the difference between GPR at points *A* and *B*, and V_ℓ is the induced voltage along the path ℓ, computed as a line integral of the magnetic vector potential $\vec{A}$. The first term $\Delta\Phi$ is defined uniquely, but the second term V_ℓ is path-dependent.

In the example in Fig. 15, $\Delta\Phi$ is larger than the total voltage V_{AB} because $\Delta\Phi$ and V_ℓ are with opposite signs and cancels each other [39], [40]. It can be seen that different resistivity of the lower soil layer has a large influence on the frequency response of the voltages.

Fig. 16 shows results for the same cases as in Fig. 15, computed by the image model ([35], [36]). The differences between the rigorous and approximate model is large in all cases, especially in the higher range of frequencies, where the approximate model largely underestimates the voltage. The reason for much higher values of V_{AB} computed by the rigorous model in the high-frequency range are differences in computed Φ_A and Φ_B. With the approximate model $\Phi_A \approx \Phi_B$, while with the rigorous $\Phi_A > \Phi_B$, which results in larger values of $\Delta\Phi$.

Figs. 17 and 18 show transient voltage along the path ℓ for first and subsequent lightning strokes, respectively. Large differences are visible between the rigorous and approximate model, especially for the response to the subsequent lightning stroke

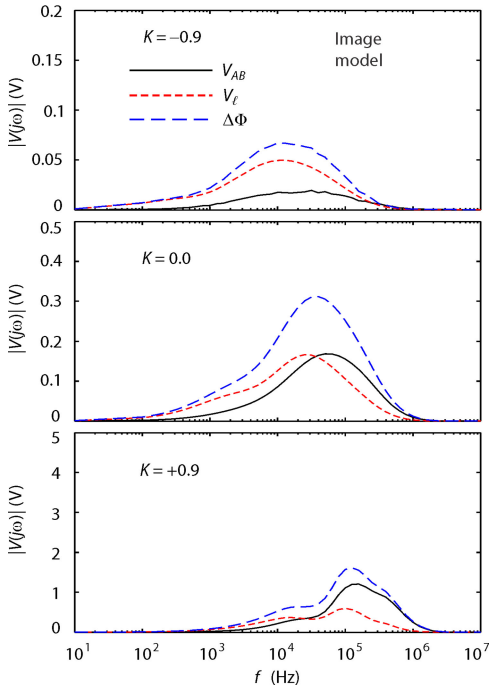

Fig. 16. Modulus of voltage along path ℓ between points A and B for three cases of two-layer soil computed by the image model.

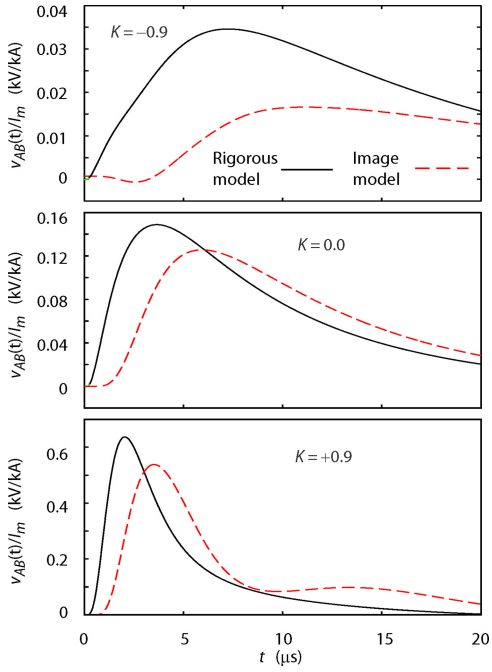

Fig. 17. Transient voltage between points A and B for the first lightning stroke ($T_1/T_2 = 8\ \mu$s/80 μs) computed by the rigorous and image model.

(Fig. 18), where the approximate model largely underestimates the peak value of the transient voltage.

Note that V_{AB} is voltage along the path of the cable when the cable is not present. However, it has been concluded that the influence of the cable might be small [34], [39], and computed V_{AB} indicates the voltage that might be coupled to the cable. An

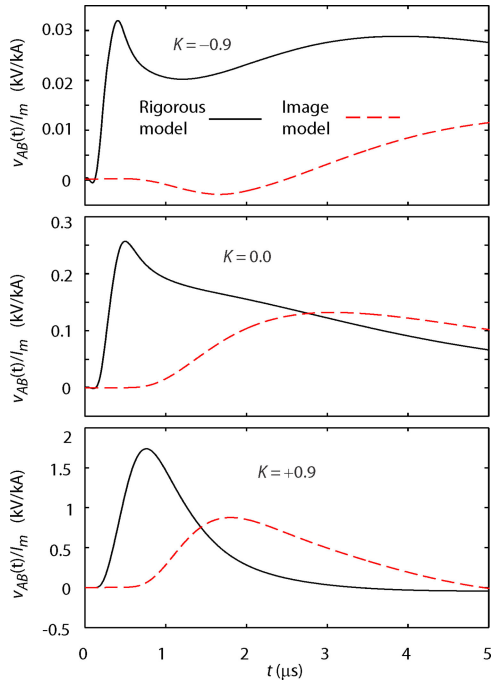

Fig. 18. Transient voltage between points A and B for the subsequent lightning stroke ($T_1/T_2 = 0.8\ \mu$s/50 μs) computed by the rigorous and image model.

analysis that includes the effect of the cable and other parameters (such as the geometry of the grid, locations of the excitation points and the path, excitation waveforms, characteristics of the soil) that influence the voltages will be considered in later work.

VIII. Conclusion

A large amount of computer time required for direct numerical integration of Sommerfeld integrals (SI), which are a key part of the rigorous electromagnetic model for transient analysis of grounding systems in multilayered soil, limits the dimensions of the system for which the method could be practically applied.

This paper presents an adaptive interpolation technique for computation of SI, which typically reduces the computation time by a factor of several tens to hundreds, maintaining a similar accuracy as the rigorous model with error limited to less than 0.1 percent. This enables the application of the rigorous method for transient analysis of very large and complex grounding systems in multilayer soil.

Presented numerical examples show an application of the developed model for computation of transient voltages that might be coupled to secondary cables in large substations. Presented results show that there are cases when approximate models based on image theory might underestimate possibly dangerous and harmful transient voltages in the case of lightning.

Appendix
Components of the Green's Functions

For convenience, only the components of the Green's functions when the source and observation points are both in the *i-th* layer are given. Details about other cases can be found

elsewhere [26], [43]. As a result of the singularity extraction procedure, Green's functions for potentials in the spatial domain are formulated in two terms, the first term expressed in closed form and the second in integral form:

$$G_A^{xx} = G_{A(CF)}^{xx} + \int_0^\infty \tilde{G}_A^{xx} J_0\left(k_\rho \rho\right) k_\rho dk_\rho \tag{7}$$

$$\frac{G_A^{zx}}{\cos\varphi} = \frac{G_A^{zy}}{\sin\varphi} = G_{A\,(CF)}^{zx/zy} + \int_0^\infty \tilde{G}_A^{zx/zy} J_1\left(k_\rho \rho\right) dk_\rho \tag{8}$$

$$\frac{K_A^{xz}}{\cos\varphi} = \frac{K_A^{yz}}{\sin\varphi} = K_{A(CF)}^{xz/yz} - \int_0^\infty \tilde{K}_A^{xz/yz} J_1\left(k_\rho \rho\right) dk_\rho \tag{9}$$

$$K_A^{zz} = K_{A(CF)}^{zz} + \int_0^\infty \tilde{K}_A^{zz} J_0\left(k_\rho \rho\right) k_\rho dk_\rho \tag{10}$$

$$G_\Phi = G_{\Phi(CF)} + \int_0^\infty \tilde{G}_\Phi\, J_0\left(k_\rho \rho\right) k_\rho dk_\rho \tag{11}$$

Spectral domain representations of the Green's functions are:

$$\tilde{G}_A^{xx} = A^{TE} \frac{e^{jk_{i,z}(z-z')}}{jk_{i,z}} + C^{TE} \frac{e^{-jk_{i,z}(z-z')}}{jk_{i,z}} \tag{12}$$

$$\begin{aligned}\tilde{G}_A^{zx/zy} = {} & (A^{TE} + B^{TM}) e^{jk_{i,z}(z-z')} \\ & + (D^{TM} - C^{TE}) e^{-jk_{i,z}(z-z')} \\ & + R_{i,i-1} e^{-jk_{i,z}h_{dn}} - R_{i,i+1} e^{-jk_{i,z}h_{up}}\end{aligned} \tag{13}$$

$$\begin{aligned}\tilde{K}_A^{xz/yz} = {} & \left(A^{TM} + B^{TE}\right) e^{jk_{i,z}(z-z')} \\ & + \left(D^{TE} - C^{TM}\right) e^{-jk_{i,z}(z-z')} \\ & + R_{i,i-1} e^{-jk_{i,z}h_{dn}} - R_{i,i+1} e^{-jk_{i,z}h_{up}}\end{aligned} \tag{14}$$

$$\begin{aligned}\tilde{K}_A^{zz} = {} & \left(2C^{TM} - D^{TE} + \frac{k_i^2}{k_\rho^2}\left(D^{TE} - C^{TM}\right)\right) \frac{e^{-jk_{i,z}(z-z')}}{jk_{i,z}} \\ & + \left(2A^{TM} + B^{TE} - \frac{k_i^2}{k_\rho^2}\left(B^{TE} + A^{TM}\right)\right) \frac{e^{jk_{i,z}(z-z')}}{jk_{i,z}} \\ & + 2\left(R_{i,i-1} \frac{e^{-jk_{i,z}h_{dn}}}{jk_{i,z}} + R_{i,i+1} \frac{e^{-jk_{i,z}h_{up}}}{jk_{i,z}}\right)\end{aligned} \tag{15}$$

$$\begin{aligned}\tilde{G}_\Phi = {} & \frac{k_{i,z}^2 B^{TM} + k_i^2 A^{TE}}{k_\rho^2} \frac{e^{jk_{i,z}(z-z')}}{jk_{i,z}} - R_{i,i-1} \frac{e^{-jk_{i,z}h_{dn}}}{jk_{i,z}} \\ & + \frac{k_i^2 C^{TE} - k_{i,z}^2 D^{TM}}{k_\rho^2} \frac{e^{-jk_{i,z}(z-z')}}{jk_{i,z}} - R_{i,i+1} \frac{e^{-jk_{i,z}h_{up}}}{jk_{i,z}}\end{aligned} \tag{16}$$

where:

$$\begin{aligned}A^{TE/TM} = {} & \tilde{R}_{i,i-1}^{TE/TM} e^{-jk_{i,z}(d_i - (z'+h_i))} \\ & \left[e^{-jk_{i,z}(d_i-(z'+h_i))} + \tilde{R}_{i,i+1}^{TE/TM} e^{-jk_{i,z}(d_i+(z'+h_i))}\right] \tilde{M}_i^{TE/TM}\end{aligned} \tag{17}$$

$$\begin{aligned}B^{TE/TM} = {} & \tilde{R}_{i,i-1}^{TE/TM} e^{-jk_{i,z}(d_i - (z'+h_i))} \\ & \left[e^{-jk_{i,z}(d_i-(z'+h_i))} - \tilde{R}_{i,i+1}^{TE/TM} e^{-jk_{i,z}(d_i+(z'+h_i))}\right] \tilde{M}_i^{TE/TM}\end{aligned} \tag{18}$$

$$\begin{aligned}C^{TE/TM} = {} & \tilde{R}_{i,i+1}^{TE/TM} e^{-jk_{i,z}(z'+h_i)} \\ & \left[e^{-jk_{i,z}(z'+h_i)} + \tilde{R}_{i,i-1}^{TE/TM} e^{-jk_{i,z}(2d_i-(z'+h_i))}\right] \tilde{M}_i^{TE/TM}\end{aligned} \tag{19}$$

$$\begin{aligned}D^{TE/TM} = {} & \tilde{R}_{i,i+1}^{TE/TM} e^{-jk_{i,z}(z'+h_i)} \\ & \left[-e^{-jk_{i,z}(z'+h_i)} + \tilde{R}_{i,i-1}^{TE/TM} e^{-jk_{i,z}(2d_i-(z'+h_i))}\right] \tilde{M}_i^{TE/TM}\end{aligned} \tag{20}$$

$$\tilde{M}_i^{TE/TM} = \left[1 - \tilde{R}_{i,i-1}^{TE/TM} \tilde{R}_{i,i+1}^{TE/TM} e^{-jk_{i,z}2d_i}\right]^{-1} \tag{21}$$

$$\tilde{R}_{i,i\pm1}^{TE/TM} = \frac{R_{i,i\pm1}^{TE/TM} + \tilde{R}_{i\pm1,i\pm2}^{TE/TM} e^{-jk_{i\pm1,z}2d_{i\pm1}}}{1 + R_{i,i\pm1}^{TE/TM} \tilde{R}_{i\pm1,i\pm2}^{TE/TM} e^{-jk_{i\pm1,z}2d_{i\pm1}}} \tag{22}$$

$$\underline{\sigma}_i = \sigma_i + j\omega\varepsilon_i, k_i = \sqrt{-j\omega\mu_0\underline{\sigma}_i}, k_{i,z} = \sqrt{k_i^2 - k_\rho^2}$$

The terms of Green's functions expressed in closed form are:

$$G_{A(CF)}^{xx} = g_{dir} \tag{23}$$

$$G_{A(CF)}^{zx/zy} = -R_{i,i-1}\hat{g}_{dn} + R_{i,i+1}\hat{g}_{up} \tag{24}$$

$$K_{A(CF)}^{xz,yz} = R_{i,i-1}\hat{g}_{dn} - R_{i,i+1}\hat{g}_{up} \tag{25}$$

$$K_{A(CF)}^{zz} = g_{dir} - 2R_{i,i-1}g_{dn} - 2R_{i,i+1}g_{up} \tag{26}$$

$$G_{\Phi(CF)} = g_{dir} + R_{i,i-1}g_{dn} + R_{i,i+1}g_{up} \tag{27}$$

$$R_{i,i\pm1} = \frac{\underline{\sigma}_i - \underline{\sigma}_{i\pm1}}{\underline{\sigma}_i + \underline{\sigma}_{i\pm1}} \tag{28}$$

$$g_{dir/up/dn} = \frac{e^{-jk_i r_{dir/up/dn}}}{r_{dir/up/dn}} \tag{29}$$

$$\hat{g}_{dir/up/dn} = \frac{1}{\rho}\left(e^{-jk_i h_{dir/up/dn}} - \frac{e^{-jk_i r_{dir/up/dn}}}{r_{dir/up/dn}} h_{dir/up/dn}\right) \tag{30}$$

$$r_{dir/up/dn} = \sqrt{\rho^2 + h_{dir/up/dn}^2}, h_{dir} = |z - z'|$$

$$h_{up} = \left|2h_i + (z + z')\right|, h_{dn} = \left|-2h_{i-1} - (z + z')\right|$$

Geometrical quantities ρ, z, z', d_i and φ are illustrated in Figs. 1 and 2.

REFERENCES

[1] *IEEE Guide for Safety in AC Substation Grounding*, IEEE Std. 80-2013, Dec. 2013.

[2] D. Roubertou, J. Fontaine, J. P. Plumey, and A. Zeddam, "Harmonic input impedance of earth connections," in *Proc. IEEE Int. Symp. Electromagn. Compat.*, 1984, pp. 717–720.

[3] L. Grcev and Z. Haznadar, "A novel technique of numerical modelling of impulse current distribution in grounding systems," in *Proc. Int. Conf. Lightning Protection*, Graz, Austria, 1988, pp. 165–169.

[4] L. Grcev and F. Dawalibi, "An electromagnetic model for transients in grounding systems," *IEEE Trans. Power Del.*, vol. 5, no. 2, pp. 1773–1781, Oct. 1990.

[5] R. Olsen and M. C. Willis, "A comparison of exact and quasi-static methods for evaluating grounding systems at high frequencies," *IEEE Trans. Power Del.*, vol. 11, no. 3, pp. 1071–1081, Jul. 1996.

[6] B. Nekhoul, C. Guerin, P. Labie, G. Meunier, R. Feuillet, and X. Brunotte, "A finite element method for calculating the electromagnetic fields generated by substation grounding systems," *IEEE Trans. Magn.*, vol. 31, no. 3, pp. 2150–2153, May 1995.

[7] M. Tsumura, Y. Baba, N. Nagaoka, and A. Ametani, "FDTD simulation of a horizontal grounding electrode and modeling of its equivalent circuit," *IEEE Trans. Electromagn. Compat.*, vol. 48, no. 4, pp. 817–825, Nov. 2006.

[8] M. Heimbach and L. Grcev, "Grounding system analysis in transients programs applying electromagnetic field approach," *IEEE Trans. Power Del.*, vol. 12, no. 1, pp. 186–193, Jan. 1997.

[9] C. L. Bak, K. E. Einarsdóttir, E. Andresson, J. M. Rasmussen, J. Lykkegaard, and W. Wiechowski, "Overvoltage protection of large power transformers—A real-life study case," *IEEE Trans. Power Del.*, vol. 23, no. 2, pp. 657–666, Apr. 2008.

[10] M. Popov, L. Grcev, H. K. Høidalen, B. Gustavsen, and V. Terzija, "Investigation of the overvoltage and fast transient phenomena on transformer terminals by taking into account the grounding effects," *IEEE Trans. Industry Appl.*, vol. 51, no. 6, pp. 5218–5227, Nov./Dec. 2015.

[11] R. F. Harrington, *Field Computation by Moment Methods*. Piscataway, NJ, USA: IEEE Press, 1993.

[12] A. Sommerfeld, *Partial Differential Equations in Physics*. New York: Academic, 1949.

[13] A. Banos, *Dipole Radiation in the Presence of a Conducting Half-Space*. Oxford, U.K.: Pergamon, 1966.

[14] L. Grcev and V Arnautovski, "Comparison between simulation and measurement of frequency dependent and transient characteristics of power transmission line grounding," in *Proc. Int. Conf. Lightning Protect*, Birmingham, U.K., 1998, pp. 524–529.

[15] L. Grcev, "Time- and frequency-dependent lightning surge characteristics of grounding electrodes," *IEEE Trans. Power Del.*, vol. 24, no. 4, pp. 2186–2196, Oct. 2009.

[16] R. G. Olsen and L. Grcev, "Analysis of high-frequency grounds: Comparison of theory and experiment," *IEEE Trans. Ind. Appl.*, vol. 51, no. 6, pp. 4889–4899, Nov./Dec. 2015.

[17] L. Grcev, "Computer analysis of transient voltages in large grounding systems," *IEEE Trans. Power Del.*, vol. 11, no. 2, pp. 815–823, Apr. 1996.

[18] F. Dawalibi, J. Ma, and R. Southey, "Behavior of grounding systems in multilayer soils: A parametric analysis," *IEEE Trans. Power Del.*, vol. 9, no. 1, pp. 334–342, Jan. 1994

[19] V. Arnautovski-Toseva, L. Grcev, "Electromagnetic analysis of horizontal wire in two-layered soil," *J. Comput. Appl. Math.* vol. 168, no. 1–2, pp. 21–29, Jul. 2004.

[20] S. Fortin, Y. Yang, J. Ma, and F. Dawalibi, "Electromagnetic fields of energized conductors in multilayer medium with recursive methodology," in *Proc. Asia-Pacific Power Energy Eng. Conf.*, 2009, pp. 1–4.

[21] H. Karami, K. Sheshyekani, and F. Rachidi, "Mixed-potential integral equation for full-wave modeling of grounding systems buried in a lossy multilayer stratified ground," *IEEE Trans. Electromagn. Compat.*, vol. 59, no. 5, pp. 1505–1513, Oct. 2017.

[22] G. Burke and E. K. Miller, "Modeling antennas near to and penetrating a lossy interface," *IEEE Trans. Antennas Propag.*, vol. AP-32, no. 10, pp. 1040–1049, Oct. 1984.

[23] P. Gay-Balmaz and J. R. Mosig, "Three-dimensional planar radiating structures in stratified media," *Int. J. Microw. Millimeter-Wave Comput.-Aided Eng.*, vol. 7, no. 5, pp. 330–343, Sep. 1997.

[24] J. Chen, A. A. Kishk, and A. W. Glisson, "A 3D interpolation model for the calculation of the Sommerfeld integrals to analyze dielectric resonators in a multilayered medium," *Electromagnetics*, vol. 20, no. 1, pp. 1–15, 2000.

[25] K. A. Michalski, "The mixed-potential electric field integral equation for objects in layered media," *Arch. Elek. Ubertragung.*, vol. 39, no. 5, pp. 317–322, Sep./Oct. 1985.

[26] K. A. Michalski and D. Zheng, "Electromagnetic scattering and radiation by surfaces of arbitrary shape in layered media, Part I: Theory," *IEEE Trans. Antennas Propagat.*, vol. 38, no. 3, pp. 335–344, Mar. 1990.

[27] R. F. Harrington, "Matrix methods for field problems," *Proc. IEEE*, vol. 55, no. 2, pp. 136–149, Feb. 1967.

[28] L. Grcev, A. Kuhar, V. A. -Toseva, and B. Markovski, "Evaluation of high-frequency circuit models for horizontal and vertical grounding electrodes," *IEEE Trans. Power Del.*, vol. 33, no. 6, pp. 3065–3074, Dec. 2018.

[29] L. Grcev, A. Kuhar, B. Markovski, and V. A. -Toseva, "Generalized network model for energization of grounding electrodes," *IEEE Trans. Electromagn. Compat.*, vol. 61, no. 4, pp. 1082–1090, Aug. 2019.

[30] A. Poggio, R. Bevensee, and E. K. Miller, "Evaluation of some thin wire computer programs," in *Proc. IEEE Antennas Propag. Symp.*, 1974, vol. 12, pp. 181–184.

[31] EM Software and Systems-S.A. (Pty) Ltd., FEKO, Stellenbosch, South Africa, [Online]. Available: http://www.feko.info

[32] B. Merheim, "Modellierung von hochspannungs-erdersystemen und vergleich mit messungen ihres dynamischen verhaltens," (in English), Dipl.Ing. thesis, Diplomaufgabe, Inst. Allgemeine ochspannungstechnik, Technischen Hochschule, Aachen, Germany, 1992.

[33] H. Rochereau and B. Merheim, "Application of the transmission lines theory and EMTP program for modelisation of grounding systems in high frequency range," in *Collection de notes internes de la Direction des Etudes et Recherches Electricité de France*, vol. 93NR00059, pp. 1–31, May 1993.

[34] B. Zhang, X. Cui, Z. Zhao, J. He, and L. Li, "Numerical analysis of the influence between large grounding grids and two-end grounded cables by the moment method coupled with circuit equations," *IEEE Trans. Power Del.*, vol. 20, no. 2, Apr. 2005, Art. no. 7310737.

[35] V. Arnautovski-Toseva and L. Grcev, "Image and exact models of a vertical wire penetrating a two-layered earth," *IEEE Trans. Electromagn. Compat.*, vol. 53, no. 4, pp. 968–976, Nov. 2011.

[36] V. Arnautovski-Toseva and L. Grcev, "On the image model of a buried horizontal wire," *IEEE Trans. Electromagn. Compat.*, vol. 58, no. 1, pp. 278–286, Feb. 2016.

[37] F. Rachidi *et al.*, "Current and electromagnetic field associated with lightning-return strokes to tall towers," *IEEE Trans. Electromagn. Compat.*, vol. 43, no. 3, pp. 356–367, Aug. 2001.

[38] K. Berger, R. B. Anderson, and H. Kroninger, "Parameters of lightning flashes," *Electra*, vol. 41, pp. 23–37, 1975.

[39] L. Grcev, "Transient voltages coupling to shielded cables connected to large substation earthing systems due to lightning," presented at the CIGRE Session, Paris, France, 1996, paper 36-301. [Online]. Available: https://e-cigre.org/publication/36-201_1996-transient-voltages-coupling-to-shielded-cables-connected-to-large-substation-earthing-systems-due-to-lightning

[40] EMC within power plants and substations. Tech. Brochure 535. Paris, France: CIGRÉ, Apr. 2013.

[41] H. Karami and K. Sheshyekani, "Harmonic impedance of grounding electrodes buried in a horizontally stratified multilayer ground: A full-wave approach," *IEEE Trans. Electromagn. Compat.*, vol. 60, no. 4, pp. 899–906, Aug. 2018.

[42] L. Grcev and M. Heimbach, "Frequency dependent and transient characteristics of substation grounding systems," *IEEE Trans. Power Del.*, vol. 12, no. 1, pp. 172–178, Jan. 1997.

[43] B. Markovski, "Efficient electromagnetic model for transient analysis of large grounding systems in layered earth," PhD Dissertation, Ss. Cyril and Methodius University in Skopje, Skopje, Macedonia, 2019.